Proceedings of ASME Turbo Expo 2016: Turbomachinery Technical Conference and Exposition
GT2016
June 13-17, 2016, Seoul, South Korea

DOI: 10.1115/GT2016-57524

GT2016-57524

ANALYTIC ASSESSMENT OF AN EMBEDDED AIRCRAFT PROPULSION

Peter F. Pelz *
Ferdinand-J. Cloos
Chair of Fluid Systems
Technische Universität Darmstadt
Darmstadt, Hesse, 64289
Germany
peter.pelz@fst.tu-darmstadt.de

Jörg Sieber
MTU Aero Engines AG
München, Bavaria, 80995
Germany
joerg.sieber@mtu.de

ABSTRACT

This paper investigates analytically the advantage of the embedded propulsion compared to a state of the art propulsion of an aircraft. Hereby, we are applying the integral method of boundary layer theory and potential theory to analyse the boundary layer thickness and the impact of the flow acceleration due to the embedded propulsion. The aircraft body is treated as a flat plate. The engine is treated as a momentum disc but there is a trade off, since the engine efficiency is effected by the boundary layer. The outcome of the energetic assessment is the following: the propulsion efficiency is increased by the embedded propulsion and the drag of the aircraft body is reduced. The optimized aircraft engine size depending on Reynolds number is given.

NOMENCLATURE

a Induction factor.
A Area.
c Absolute velocity.
c_f Friction coefficient.
c'_f Local friction coefficient.
C Constant.
$\vec{e}_x$ Unit vector in x-direction.
f_+ Friction coefficient.
H Stream tube height.
L Aircraft body length.
n Exponent of the velocity power law.
p Pressure.
P_s Shaft power.
R Gas constant.
Re Reynolds number.
S Thrust.
$\vec{t}$ Stress vector.
T Temperature.
u Flow velocity within the boundary layer.
u_* Friction velocity.
U Flow velocity outside the boundary layer.
v Flying speed.
W_0 Body drag force.
W_f Friction force.
x Axial coordinate.
y Wall coordinate.
α_p Shaft power ratio.
α_w Friction force ratio.
γ Isentropic exponent.
δ Boundary layer thickness.
δ_1 Displacement boundary layer thickness.
δ_2 Momentum boundary layer thickness.
ζ Dimensionless constant.
η Efficiency.
η_{Fr} Propulsion efficiency (Froud).
κ Slenderness ratio.
κ_1 Dimensionless constant.

*Address all correspondence to this author.

κ_2 Dimensionless constant.
λ Dimensionless constant.
ν Kinematic viscosity.
ρ Air density.
τ_w Wall shear stress.
ϕ Flow potential.

INTRODUCTION

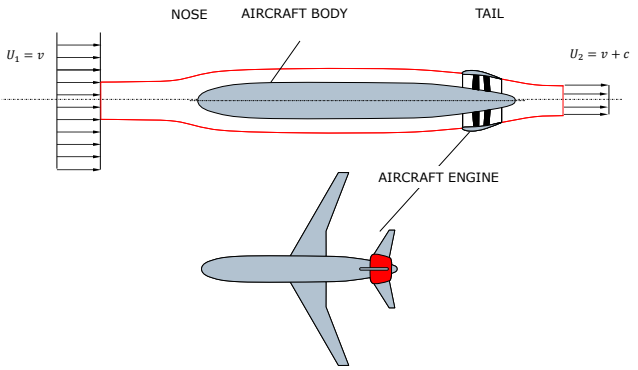

FIGURE 1. EMBEDDED PROPULSION OF AN AIRCRAFT.

Figure 1 shows an aircraft engine embedded in the aircraft body. This set-up is one possibility among others of an embedded propulsion. For this topology there are two contradicting influences: first, the friction resistance W_f of the hull will be reduced due to the boundary layer acceleration. Second, the engine efficiency will be negative effected due to the non-uniform velocity profile at the engine inlet. Both effects are contradicting and can be traced back to the boundary layer thickness δ. For the first effect, the ratio of δ to hull length L will be important. For the second effect, the ratio of δ to the engine size H is relevant. Hence, we expect an optimal slenderness ratio $\kappa := H/L$ as a function of the Reynolds number for the minimal power consumption. This paper discusses the aerodynamic advantage of the embedded propulsion compared to an conventional propulsion by propulsion efficiency analysis. The influence of the propulsion interacting with the boundary layer is investigated by Tillman, Hardin et al. [1, 2]. For different aircraft configurations the power balance method for performance estimation is applied by Sato [3] and Drela [4].

The aircraft body is treated as a flat plate. Following the idea of Rankine 1865 [5] and Betz [6] the aircraft engine is modelled as a disc actuator. This approach is only valid for propeller engines. Thus, this analysis neglects the fuel mass flow and the flow is assumed to be incompressible. An extension to a compressible flow of the present theory is possible. Thus, the principle approach does not change for a compressible flow. By doing so, we yield two configurations; see Fig. 2. For the conventional propulsion representing the reference case, a pylon connects the aircraft engine with the aircraft body. For the embedded propulsion the aircraft engine is embedded in the aircraft body.

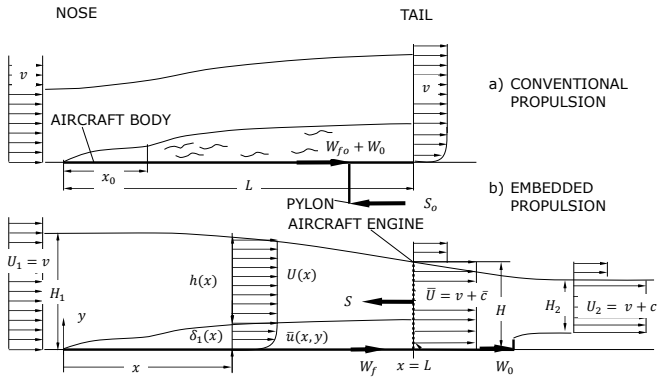

FIGURE 2. SCHEMATICAL DESCRIPTION OF THE BOUNDARY LAYER AND STREAM TUBE FOR a) THE CONVENTIONAL AND b) THE EMBEDDED PROPULSION.

This paper is organized as follows: first, we discuss the axial momentum balance and we introduce the axial induction factors $a := c/v$ and $\bar{a} := \bar{c}/v$. Second, the outer flow will be discussed by potential theory. By the third step, we calculate the boundary layer thickness, e.g. the friction drag, with the results from the previous sections and compare the embedded propulsion with the conventional propulsion. At last, the first law of thermodynamics is applied to define the efficiency. By doing so, the optimal engine size is given by the shaft power ratio of the two topologies. In the closure of this paper, we summarize our investigation by three major findings.

AXIAL MOMENTUM BALANCE

For the embedded propulsion the axial momentum balance reads

$$\int_0^H \rho \overline{u}^2 \mathrm{d}y - \rho U_1 \overline{U} H = W_f - p_1 H, \tag{1}$$

with the pressure p_1 in front of the disc, the velocities u and U, the height H and the air density ρ. The friction force is

$$W_f = \vec{e}_x \cdot \int_{A_k} \vec{t}\, \mathrm{d}A, \tag{2}$$

with A_k the wetted area of the whole aircraft body. Using the displacement thickness δ_1, defined as usual as

$$\delta_1 := \int_0^\infty \left(1 - \frac{\overline{u}}{U}\right) \mathrm{d}y \tag{3}$$

and the momentum thickness

$$\delta_2 := \int_0^\infty \left(1 - \frac{\overline{u}}{U}\right) \frac{\overline{u}}{U} \mathrm{d}y, \tag{4}$$

the left side of Eqn. 1 yields

$$\int_0^H \rho \overline{u}^2 \mathrm{d}y - \rho U_1 \overline{U} H = \rho U^2 (H - \delta_1 - \delta_2) - \rho U_1 \overline{U} H, \tag{5}$$

evaluated in front of the disc at $x = L$.

The continuity equation reads

$$\overline{U} H - \int_0^H \overline{u} \, \mathrm{d}y = \overline{U} H - (H - \delta_1) U = 0 \tag{6}$$

at the disc and with the Bernoulli equation

$$p_1 = -\frac{\rho}{2} \left(U^2 - U_1^2\right) \tag{7}$$

for the pressure in front of the disc, the axial momentum balance yields

$$\overline{U}^2 \lambda - 2v\overline{U} + v^2 = \frac{2W_f}{\rho} \tag{8}$$

with

$$\lambda := \frac{H^2 - 2H(\delta_1 + \delta_2)}{(H - \delta_1)^2} = 1 - 2\delta_{2+}. \tag{9}$$

δ_{2+} is approximately the dimensionless momentum thickness neglecting terms higher order, thus

$$\delta_{2+} \approx \frac{\delta_2}{H}. \tag{10}$$

Following the nomenclature of Glauert [7], the ratio of the total jet velocity and the velocity of transport, e.g. flying speed, is

$$a := \frac{c}{v} = \frac{U_2}{v} - 1, \tag{11}$$

the so called axial induction factor of the disc. Close to the disc, the induction factor is definded as

$$\overline{a} := \frac{\overline{c}}{v} = \frac{\overline{U}}{v} - 1. \tag{12}$$

With the induction factors, the friction coefficients

$$c_f := \frac{2W_f}{\rho v^2 L}, \tag{13}$$

$$f_+ := \frac{c_f}{\kappa}, \tag{14}$$

and the slenderness ratio

$$\kappa := \frac{H}{L}, \tag{15}$$

we obtain

$$(\overline{a} + 1)^2 \lambda - 2\overline{a} = f_+ + 1. \tag{16}$$

The axial momentum balance for the stream tube from the beginning of the aircraft body behind the disc for the induction factors $\overline{a}$ and a, reads

$$\rho H \overline{U} \left(\overline{U} - U_1\right) = S - p_2 H, \tag{17}$$

with the pressure p_2 behind the disc. The thrust S equals the sum of the friction force W_f and body drag W_0 at constant flying speed v

$$S = W_f + W_0. \tag{18}$$

The body drag is given by

$$W_0 = \rho H \overline{U} \left(U_2 - U_1\right). \tag{19}$$

Using Bernoulli's equation behind the disc to the free jet stream, the pressure behind the disc is

$$p_2 = \frac{\rho}{2}\left(U_2^2 - \overline{U}^2\right). \tag{20}$$

Following the nomenclature of Glauert, Eqn. 17 yields

$$(\overline{a} - a)^2 = f_+, \tag{21}$$

thus, the induction factor a is given by

$$a = \sqrt{f_+} + \overline{a}. \tag{22}$$

With Eqn. 16 and 22 the induction factors $a(\delta_+, f_+)$ and $\overline{a}(\delta_+, f_+)$ are given. A reference case without a boundary layer, e.g. $\delta_+ = 0$ and $\lambda = 1$, the well known Betz solution $\overline{a} = 1/2a$ is included. For the general case, the induction factors $a(\delta_+, f_+)$ and $\overline{a}(\delta_+, f_+)$ are given by Fig. 3 and 4, respectively.

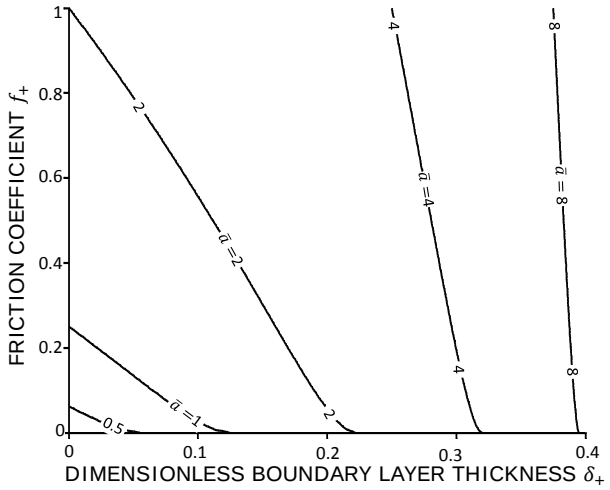

FIGURE 3. INDUCTION FACTOR $\overline{a}$ DEPENDENT ON BOUNDARY LAYER THICKNESS AND FRICTION COEFFICIENT.

Figure 5 shows the ratio $\overline{a}/a$ of the induction factors. The solid line indicates the Betz solution for $\delta_+ = 0$ and the dashed line indicates $2\delta_+ = f_+$; the solution for a constant pressure boundary layer as we will show in the following sections.

For a compressible flow Eqn. 20 has to be replaced by $u/2 + \gamma/(\gamma - 1)\ p/\rho = \text{const.}$. As usual the equation of state $p = \rho RT$ is as well needed as well as the energy equation in integral form [8,9].

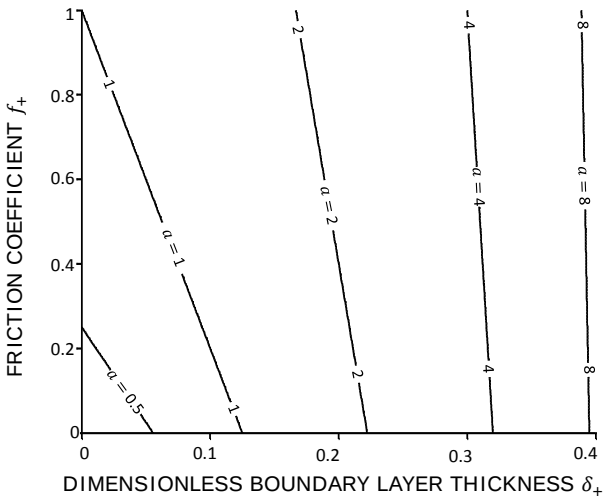

FIGURE 4. INDUCTION FACTOR a DEPENDENT ON BOUNDARY LAYER THICKNESS AND FRICTION COEFFICIENT.

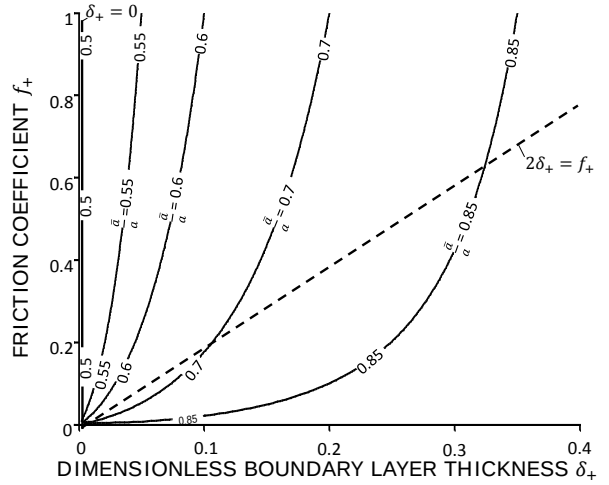

FIGURE 5. INDUCTION FACTORS RATIO $\overline{a}/a$ DEPENDENT ON BOUNDARY LAYER THICKNESS AND FRICTION COEFFICIENT. THICK SOLID LINE INDICATES $\delta_+ = 0$, DASHED LINE $2\delta_+ = f_+$.

OUTER FLOW

Outside the boundary layer, e.g. the outer flow, the flow is irrotational. There, the velocity field is given by $\vec{U} = \nabla\phi$. The flow upstream of the disc is described by a superposition of the following three sections: first, the potential of undisturbed approaching flow $U_1 x$. Second, the line sink at $x = L$, $-H < y' < H$ with the sink strength $-4\overline{c}H$. Third, the combination of sinks and sources to consider the boundary layer at the

flat plate. Thus, we obtain

$$\begin{aligned}\phi =& U_1 x - \frac{\overline{c}}{\pi}\int_{-H}^{H} \ln\sqrt{(x-L)^2+(y-y')^2}\,\mathrm{d}y + \ldots \\ &+ \int_0^L \frac{U(x')}{\pi}\frac{\mathrm{d}\delta_1(x')}{\mathrm{d}x'}\ln\sqrt{(x-x')^2+y^2}\,\mathrm{d}x.\end{aligned} \tag{23}$$

The velocity of the outer flow is given by

$$U(x) = \left.\frac{\partial\phi}{\partial x}\right|_{y=\delta(x)}. \tag{24}$$

The displacement of the boundary layer influences the velocity less than the propulsion does. Thus, the second term on the ride side of Eqn. 23 for the velocity profile within the boundary layer is negligible. The velocity of the outer flow

$$\frac{U(x)}{U_1} \approx 1 - \frac{\overline{a}}{\pi}\int_{-H}^{H}\frac{x-L}{(x-L)^2+y'^2}\,\mathrm{d}y' \tag{25}$$

depends on the induction factor.

BOUNDARY LAYER AND DRAG

Figure 2 illustrates the boundary layer at the flat plate, e.g. the aircraft body. The drag force is the sum of friction force and body drag; see Eqn. 18. The friction force is the integral of the wall shear stress

$$W_f = \int_0^L \tau_w\,\mathrm{d}x. \tag{26}$$

The wall shear stress is $\tau_w := \rho u_*^2$ with the friction velocity u_* and yielding the local friction coefficient

$$c_f' := \frac{2\tau_w}{\rho U^2} = 2\frac{u_*^2}{U^2}. \tag{27}$$

Hence, the friction force is

$$c_f := \frac{2W_f}{\rho U_1^2 L} = \frac{1}{L}\int_0^L \left(\frac{U}{U_1}\right)^2 c_f'\,\mathrm{d}x. \tag{28}$$

With the integral method of the boundary layer theory and Eqn. 3 and 4, the axial momentum balance is

$$\frac{\mathrm{d}\delta_2}{\mathrm{d}x} + \frac{1}{U}\frac{\mathrm{d}U}{\mathrm{d}x}(2\delta_2+\delta_1) = \frac{\tau_w}{\rho U^2} = \frac{u_*^2}{U^2} = \frac{c_f'}{2}, \tag{29}$$

the so called van Kármán momemtum equation and is valid for laminar and turbulent flow.

Reference Case

The reference case, e.g. the conventional propulsion Fig. 2, has a constant pressure boundary layer, thus, $U = U_1 = \text{const.}$. Applying Eqn. 29 to the reference case, yields $2\mathrm{d}\delta_2/\mathrm{d}x = c_f'$. With an ansatz function for the axial velocity profile within the boundary layer, for example Prandtl's power law

$$u(x,y) = U(x)\left(\frac{y}{\delta(x)}\right)^n, \tag{30}$$

the friction coefficient is

$$c_{f0} = 0.072\left(\frac{U_1 L}{\nu}\right)^{-1/5} = 0.072\,Re^{-1/5}. \tag{31}$$

Equation 31 is the well known Blasius power law [10]. The solution of the integral method for boundary layer theory is very robust against assumed ansatz functions [10–12], in our case Eqn 30. Hence, to verify the ansatz function is not necessary.

Boundary Layer of the Embedded Propulsion

For the boundary layer of the embedded propulsion, we consider the outer flow solution $U(x)$, see Eqn. 25, to solve the von Kármán momentum equation (Eqn. 29). Using Eqn. 30 for the velocity profile within the boundary layer, we obtain

$$\frac{\delta_1}{\delta} := \int_0^1 \left(1-\frac{u}{U}\right)\,\mathrm{d}\left(\frac{y}{\delta}\right) = \frac{n}{n+1}, \tag{32}$$

for the displacement thickness and

$$\frac{\delta_2}{\delta} := \int_0^1 \frac{u}{U}\left(1-\frac{u}{U}\right)\,\mathrm{d}\left(\frac{y}{\delta}\right) = \frac{n}{(n+1)(2n+1)}, \tag{33}$$

for the momentum thickness. Thus, $\delta_1 = (2n+1)\delta_2 = h\delta_2$ with $h := 2n+1$. The choosen power law has to be calibrated to the

viscous sublayer [10]

$$\frac{u}{u_*} = C\left(\frac{yu_*}{\nu}\right)^n, \tag{34}$$

with the constant C. For $n = 1/7$, the empirical constant C is 8.74 [10]. Hence, the wall shear stress is

$$\tau_w = \rho\left(\frac{U\nu^n}{C\delta^n}\right)^{\frac{2}{n+1}}. \tag{35}$$

With these deviations and

$$\delta := \zeta\delta_1, \tag{36}$$

$$\zeta := \frac{(2n+1)(n+1)}{n}, \tag{37}$$

$$\kappa_1 := \frac{2n}{n+1} + 1 \tag{38}$$

and

$$\kappa_2 := \frac{2}{n+1}, \tag{39}$$

we obtain the von Kármán momentum equation for the embedded propulsion

$$\delta_2^{\kappa_1}\frac{\mathrm{d}\delta_2}{\mathrm{d}x} + \frac{1}{U}\frac{\mathrm{d}U}{\mathrm{d}x}(2+h)\,\delta_2^{\kappa_1+1} = \left[\frac{1}{CU}\left(\frac{\nu}{\zeta}\right)^n\right]^{\kappa_2}. \tag{40}$$

Hence, the momentum thickness for the embedded propulsion is

$$\delta_2(x) = 0.036\left[\nu^{\frac{1}{4}}U^{-\frac{115}{28}}\int_0^x U^{\frac{108}{28}}\,\mathrm{d}x\right]^{4/5}. \tag{41}$$

FRIST LAW OF THERMODYNAMICS AND FROUD PROPULSION EFFICIENCY

The shaft power is

$$P_s = \frac{1}{\eta}\overline{U}H\Delta p, \tag{42}$$

with the mean velocity $\overline{U}$ and the aerodynamic, e.g. isotropic, efficiency η of the embedded propulsion and η_0 of the reference case.

Propulsion Efficiency of the Reference Case

For a constant flying speed $v = U$, the shaft power for the reference case is $P_{s0} = S_0\overline{U}_0/\eta_0$ and the Froud efficiency is given by

$$\eta_{Fr,0} := \frac{S_0U_1}{P_{s0}} = \eta_0\frac{U_1}{\overline{U}} = \eta_0\frac{U_1}{U_1+\frac{c}{2}}. \tag{43}$$

This is the well known definition of the propulsion efficiency [13].

Propulsion Efficiency of the Embedded Propulsion

For the embedded propulsion we calculate the propulsion efficiency to

$$\eta_{Fr} := \frac{SU_1}{P_s} = \eta\frac{SU_1}{\overline{U}H\Delta p}, \tag{44}$$

with the thrust

$$S = H\frac{\rho}{2}\left(\overline{U}^2 - 2\overline{U}U_1 + U_2^2\right), \tag{45}$$

the pressure difference

$$\Delta p = p_2 - p_1 = \frac{\rho}{2}\left(U_2^2 - U_1^2 + 2\delta_{1+}\overline{U}^2\right) \tag{46}$$

and the dimensionless displacement thickness

$$\delta_{1+} := \frac{\delta_1}{H}\frac{1-\delta_1/(2H)}{(1-\delta_1/H)^2} \approx \frac{\delta_1}{H}. \tag{47}$$

Thus, the propulsion efficiency is

$$\frac{\eta_{Fr}}{\eta} = \frac{U_1}{\overline{U}}\frac{\overline{U}^2 - \overline{U}U_1 + U_2^2}{U_2^2 - U_1^2 + 2\delta_{1+}\overline{U}^2}. \tag{48}$$

Figure 6 shows the propulsion efficiency.

Comparing both cases, one has to noe that the friction force as well as the shaft power differ but the body drag W_0 is assumed

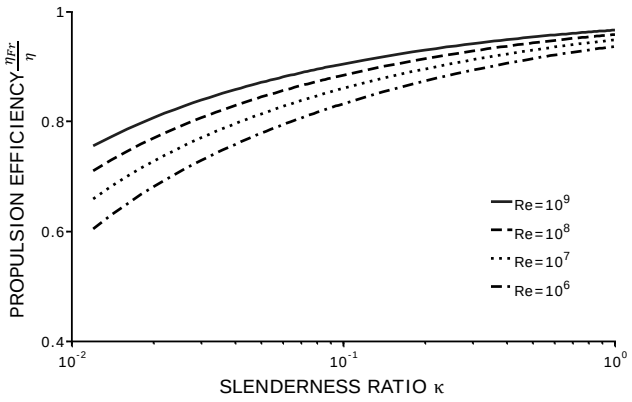

FIGURE 6. PROPULSION EFFICIENCY DEPENDENT ON SLENDERNESS RATIO κ FOR VARIOUS REYNOLDS NUMBER $Re = U_1 L/\nu$.

to be approximately constant for both cases. The friction force ratio is

$$\alpha_w := \frac{W_f}{W_{f0}} = \frac{c_f}{c_{f0}} \tag{49}$$

and is illustrated in Fig. 7. The flying speed is constant for both cases, thus the shaft power ratio is to analyse and not the propulsion efficiency. The shaft power ratio is

$$\alpha_p := \frac{P_s}{P_{s0}} = \frac{\eta_0}{\eta}\frac{\overline{U}}{\overline{U}_0}\frac{\Delta pH}{W_0 + W_{f0}} \tag{50}$$

and is shown in Fig. 8. Applying Eqn. 19, Eqn. 50 yields

$$\alpha_p = \frac{1}{2}\frac{\eta_0}{\eta}\frac{\overline{U}}{U_1 + \frac{c}{2}}\frac{U_2^2 - U_1^2 + 2\delta_{1+}\overline{U}}{\overline{U}\,(U_2 - U_1) + U_1^2 c_{f0}\frac{L}{2H}}. \tag{51}$$

Conclusion

This paper analyses the energetic assessment of two different aircraft propulsion topologies. For the first case, e.g. the reference case, the propulsion system is connect by a pylon to the aircraft body. For the second case, the propulsion system is embedded in the aircraft body. We derive the axial momentum balance for both cases including a solution for the boundary layer, e.g. the friction drag, and the outer flow. Hereby, we applied the integral method of boundary layer theory and the potential theory, respectively. The outcome of this assessment are the following three major findings:

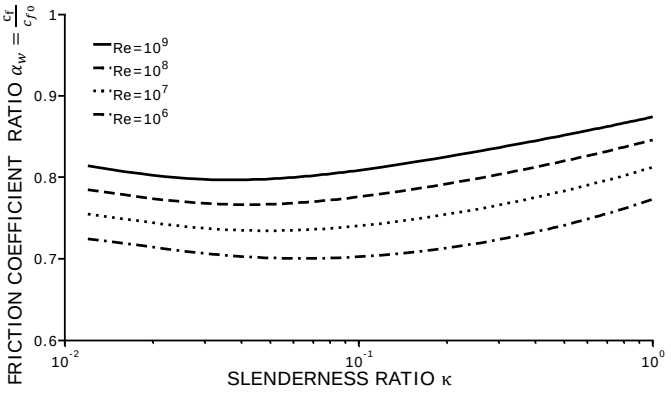

FIGURE 7. FRICTION COEFFICIENTS RATIO DEPENDENT ON SLENDERNESS RATIO FOR VARIOUS REYNOLDS NUMBER $Re = U_1 L/\nu$.

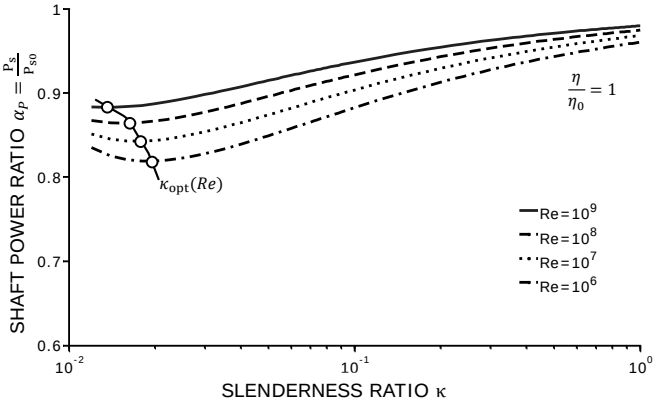

FIGURE 8. SHAFT POWER RATIO DEPENDENT ON SLENDERNESS RATIO FOR VARIOUS REYNOLDS NUMBER $Re = U_1 L/\nu$.

1. For increasing aircraft engine and increasing Reynolds number Re, the propulsion efficiency increases as well; see Fig. 6.
2. The optimized aircraft engine is given by Fig. 7. The friction force is decreased depending on Reynolds number and aircraft engine size $\kappa := H/L$.
3. The energetic improvement of the embedded propulsion is in relation to the reference case about 10 %; see Fig. 8.

References

[1] Tillman, T., Hardin, L., Moffitt, B., Sharma, O., Lord, W., Berton, J., and Arend, D., 2011. "System-level benefits of boundary layer ingesting propulsion". In Invited paper, presented at the 49th AIAA Aerospace Sciences Meeting, Orlando, FL.

[2] Hardin, L., Tillman, T., Sharma, O. P., Berton, J.,

and Arend, D. J., 2012. "Aircraft system study of boundary layer ingesting propulsion". In 48th AIAA/ASME/SAE/ASEE Joint Propulsion Conference and Exhibit.

[3] Sato, S., et al., 2012. "The power balance method for aerodynamic performance assessment". PhD thesis, Massachusetts Institute of Technology.

[4] Drela, M., 2009. "Power balance in aerodynamic flows". *AIAA journal,* ***47***(7), pp. 1761–1771.

[5] Rankine, W., 1865. "On the mechanical principles of the action of propellers". *Transactions of the Institution of Naval Architects,* ***6***, pp. 13–39.

[6] Betz, A., 1926. *Windenergie und ihre Ausnutzung durch Windmühlen*. Vandenhoeck.

[7] Glauert, H., 1929. "Grundlagen der Tragflügel- und Luftschraubentheorie (aus dem Englischen übersetzt von H. Holl)". *Julius Springer-Verlag, Berlin*.

[8] Becker, E., 1966. *Gasdynamik*, Vol. 6. Teubner.

[9] Saul, S., STONJEK, S., and Pelz, P. F., 2015. "Influence of compressibility on incidence losses of turbomachinery at subsonic operation". In International Conference on Fan Noise, Technology and Numerical Mehtods.

[10] Schlichting, H., 1970. *Boundary-Layer Theory*. McGraw Hill.

[11] Pohlhausen, K., 1921. "Zur näherungsweisen Integration der Differentialgleichung der laminaren Grenzschicht". *ZAMM,* ***1***(4), pp. 252–268.

[12] v. Kármán, T., 1921. "Über laminare und turbulente Reibung". *ZAMM,* ***1***(4), pp. 233–252.

[13] Prandtl, L., 1944. *Führer durch die Strömungslehre*. F. Vieweg & Sohn, Braunschweig.